

Self-Healable Transparent Polymer/Salt Hybrid Adhesive via Ternary Bonding Effect

Supporting Information

1. Supplemental characterization methods

The glass transition temperature of the hybrids was measured using differential scanning calorimeter (DSC, Mettler Toledo DSC 1). Approximately 5 mg samples were heated over the temperature range of 20 °C to 180 °C with a heating rate of 10 °C min⁻¹ in a nitrogen atmosphere. The moisture uptake was tested by putting the film samples into a humidity chamber with T=25 °C and RH=95% ± 2% for 24 h. The films were weighed to a precision of 0.1 mg before and after the tests. The moisture uptake percentage of the hybrids were calculated by the weight change rate using equation (1):

$$\frac{W_t - W_0}{W_0} \times 100\% \quad (1)$$

where W_t is the weight of film after 24 h-test and W_0 is the original weight of the film.

Raman spectrum was recorded by Renishaw inVia Raman spectrometer. The micro-morphology of the samples was studied by scanning electron microscope (SEM, FEI Nova NanoSEM 450). For the measurement of elemental concentration, 1.1418 g mixture of soil and plaster from ancient wall painting was dissolved in 30 mL deionized water and stirred for 24 h. After centrifugation, the supernatant was collected for further analysis. Thermo Fisher ICS-1100 ion chromatography system was adopted in the analysis of the anions' concentration. The concentration of cation elements was measured by Agilent 7700 ICP-MS MassHunter Workstation.

2. Supplemental results and discussion

The DSC was adopted to characterize the miscibility of the hybrid materials. The glass transition temperature (T_g) of a blend material indicates the miscibility of different portions. Fig. S1a shows the DSC curves of the hybrids at different PHS/PEOZ ratios, and the T_g values are recorded in Table S1. All the hybrids displayed a single T_g , which implies that the hybrids of PEOZ and PHS are in single-phase and have good miscibility.

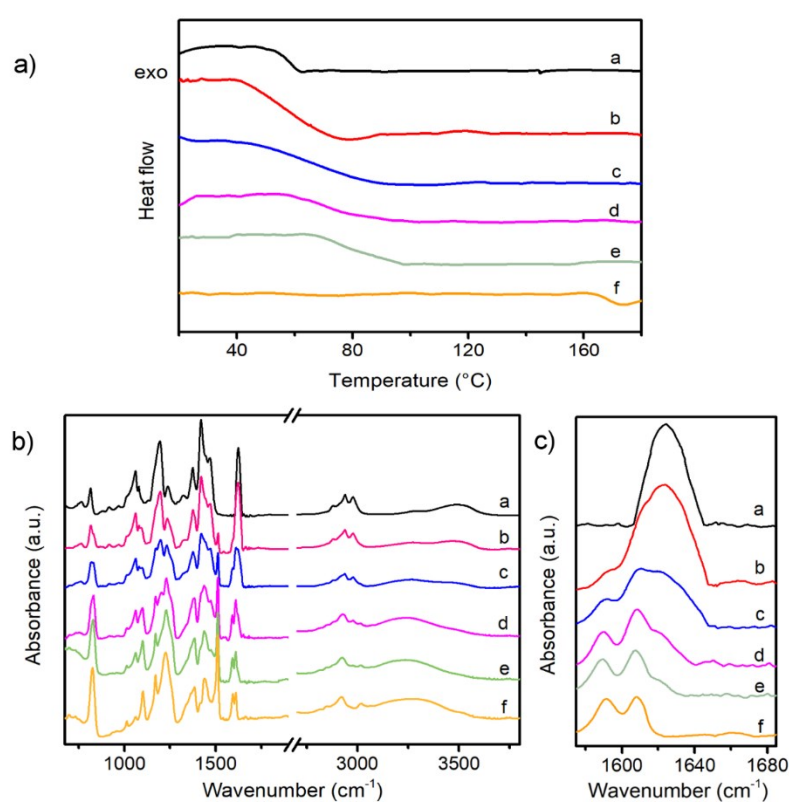


Fig. S1. Characterization of the hybrids. **a)** DSC curves of the neat polymers and hybrids. **b)** FT-IR spectra of films of neat polymers and hybrids, **c)** the peaks of carbonyl shift due to the hydrogen bonding. In each graph, **a**, **b**, **c**, **d**, **e**, and **f** refer to PEOZ, 15PHS/PEOZ, 30PHS/PEOZ, 50PHS/PEOZ, 70PHS/PEOZ, and PHS, respectively.

Table S1. The glass transition temperature of the hybrids with different PHS/PEOZ ratios.

Sample	PEOZ	15PHS/PEOZ	30PHS/PEOZ	50PHS/PEOZ	70PHS/PEOZ	PHS
T _g (°C)	56	60	70	74	81	168

Then the hybrid series were characterized by Fourier Transform Infrared Spectroscopy (FTIR) spectroscopy. The peak at 1624 cm⁻¹ is assigned to the C=O stretching band of PEOZ (Fig. S1b, curve a), and the peaks at 1591 cm⁻¹ and 1608 cm⁻¹ refer to the C=C vibration of the benzene ring of PHS¹ (Fig. S1b, curve f). There are no new chemical bonds produced within the hybrid system; therefore, PEOZ does not chemically react with PHS. As the proportion of PHS is increased, the C=O stretching band of PEOZ shifts slightly to lower wavenumber (Fig. S1c). Meanwhile, in the OH stretching region, the inter-associated O-H bond of PHS is observed at 3273 cm⁻¹ (-OH□□□HO-) of curve f. The peaks move to lower wavenumber with the increasing of PEOZ up to 50 wt% (Fig. S1b, curve d), which demonstrates that more hydroxyl groups involve in the hydrogen bonding with the carbonyl groups of PEOZ. Several reports also confirmed the hydrogen bonding site of the tertiary amide with phenol is on oxygen.²⁻⁴ And the position of this bonded -OH group remains stable with more than 70 wt% PEOZ (curve c), which means that -C=O□□□HO- is predominant in the hydrogen bonding. It is proven that PEOZ and PHS are miscible due to hydrogen bonds⁵.

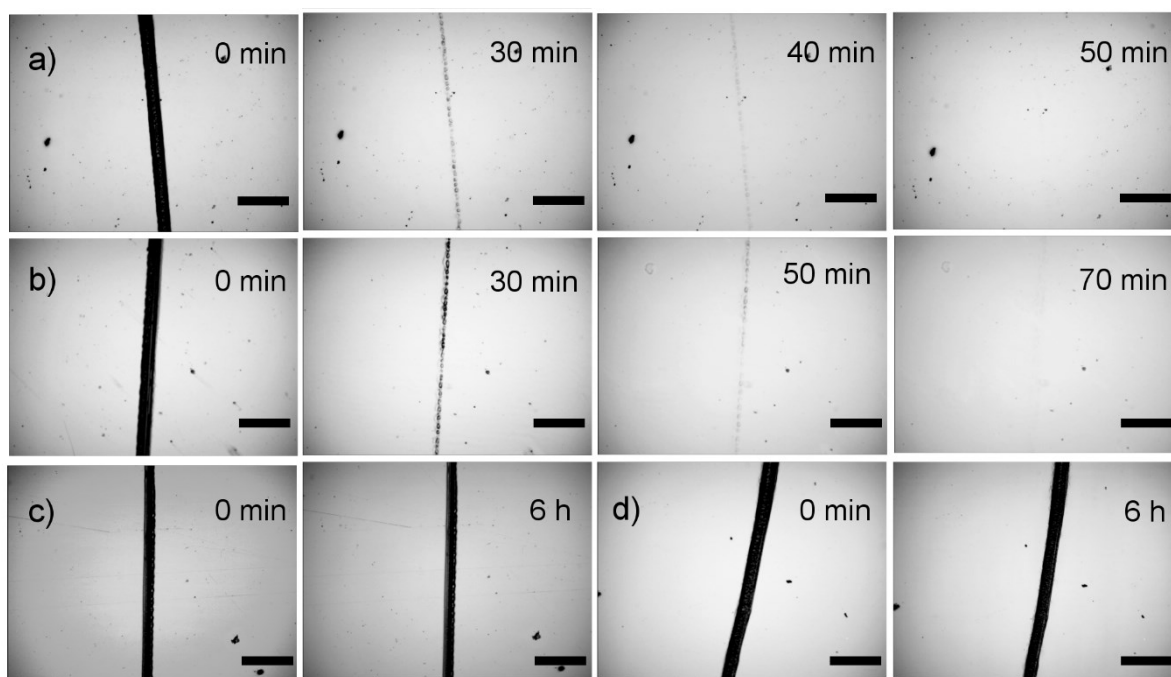


Fig. S2. Optical photographs of the self-healing process of **a)** 15PHS/PEOZ, **b)** 30PHS/PEOZ, **c)** 50PHS/PEOZ, and **d)** 70PHS/PEOZ. 50PHS/PEOZ and 70PHS/PEOZ show no self-healing ability after 6 h. Scale bar: 100 μm .

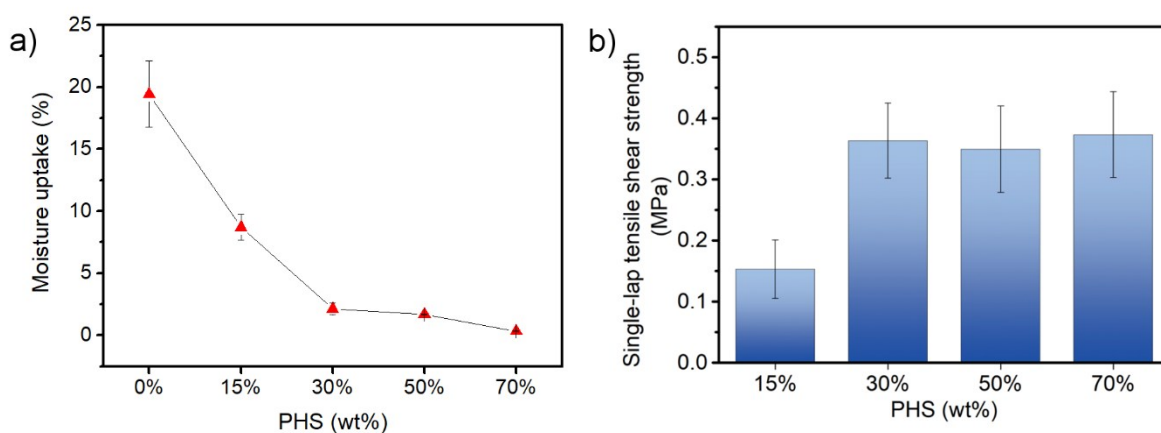


Fig. S3. Moisture uptake and adhesion strengths of the hybrid films. **a)** Moisture uptake percentage of pure PEOZ and the PHS/PEOZ hybrids. **b)** The adhesion strength of pure PEOZ and the PHS/PEOZ hybrids in the environment of $RH \approx 95\%$. Error bars are the standard deviation for five measurements.

The moisture uptake of the hybrid films was studied (Fig. S3a). PEOZ absorbs 19.43% of moisture after being put in the humidity chamber ($RH \approx 95\%$) for 24 h and becomes gel-like and sticky due to its high hydrophilicity. In comparison, the moisture up-taken of 30PHS/PEOZ decreases dramatically to 2.13%. For the hybrids of 50PHS/PEOZ and 70PHS/PEOZ, the moisture up-taken reduce to 1.68% and 0.34%, respectively. Besides, the adhesion strengths of PEOZ and the hybrids in a wet environment were tested by the single-lap tensile shear strength test (Fig. S3b). After being put in the humidity chamber ($RH \approx 95\%$) for 24 h, the pure PEOZ bonded specimens easily get separated, and the adhesion strength is only about 0.041 ± 0.016 MPa. The strength increases to 0.360 ± 0.061 MPa when the hybrid 30PHS/PEOZ is used and does not change much when more PHS is added (i.e., 50PHS/PEOZ and 70PHS/PEOZ).

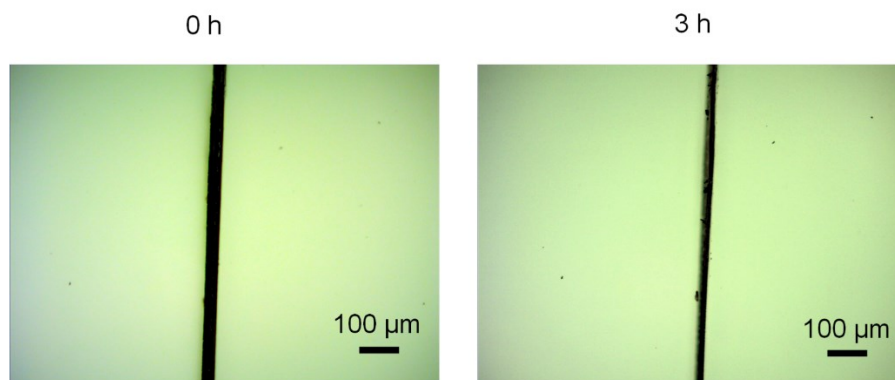


Fig. S4. Optical images of the scratch on the 30PHS/PEOZ film for the self-healing test in the environment at 35 °C, RH 54%. The film of 30PHS/PEOZ cannot heal completely in 3 h, which is longer than in the RH 95% environment (70 min). These parameter settings are as the same dew point with 25 °C, RH 95%.

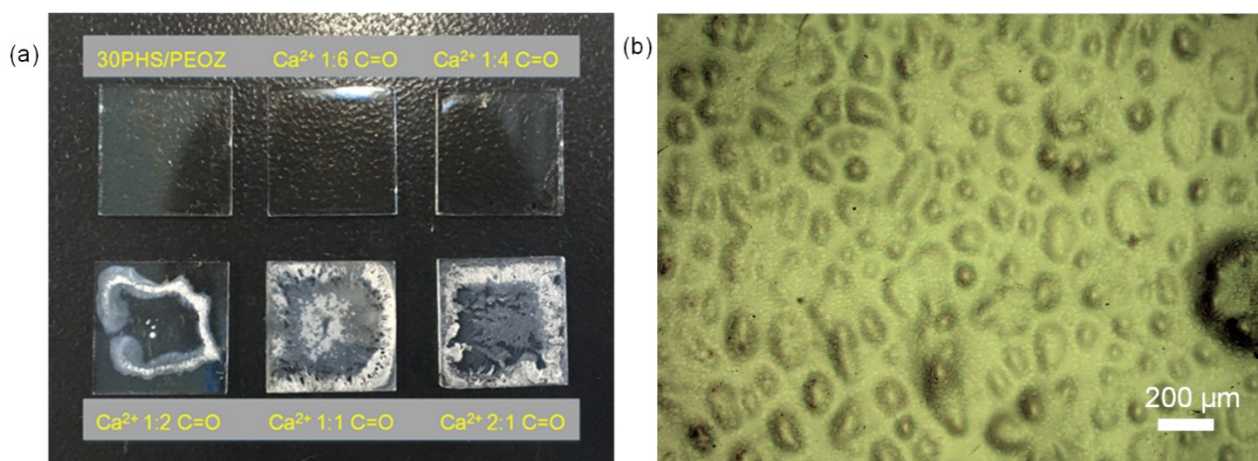


Fig. S5. (a) The overall morphologies of the 30PHS/PEOZ films and 30PHS/PEOZ blended with different ratios of CaCl_2 . (b) The optical micrograph of the film of Ca^{2+} 1: 2 C=O.

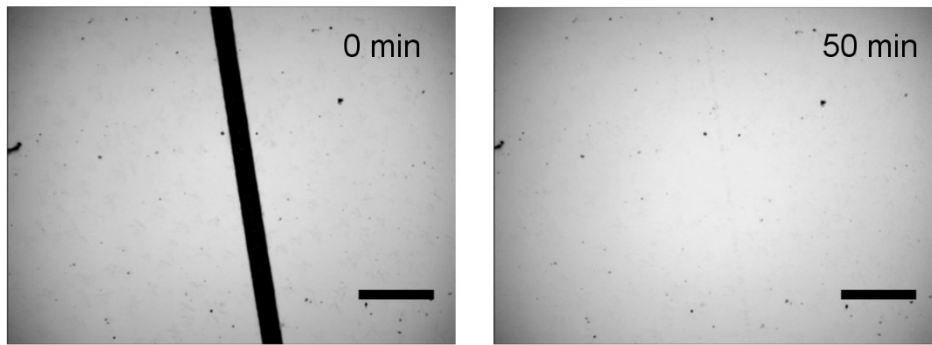


Fig. S6. Self-healing of 30PHS/PEOZ using PEOZ with $M_w \approx 10,400$. Scale bars: 100 μm .

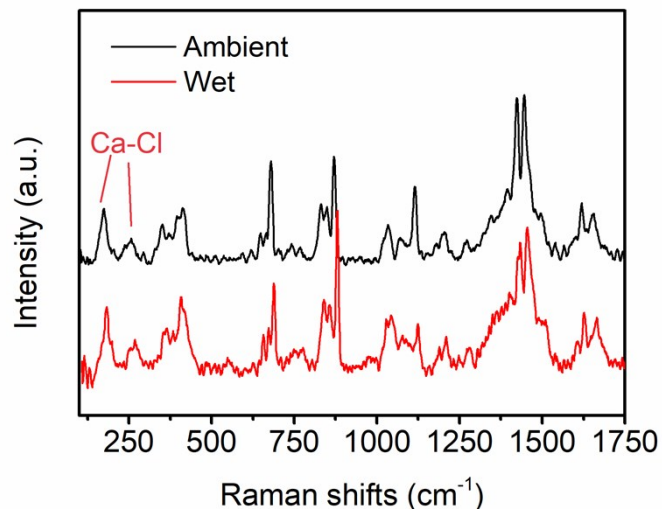


Fig. S7. The Raman spectra of 30PHS/PEOZ+CaCl₂ in both ambient and wet environments. The peaks at 171 cm^{-1} and 256 cm^{-1} correspond to Ca-Cl.⁶

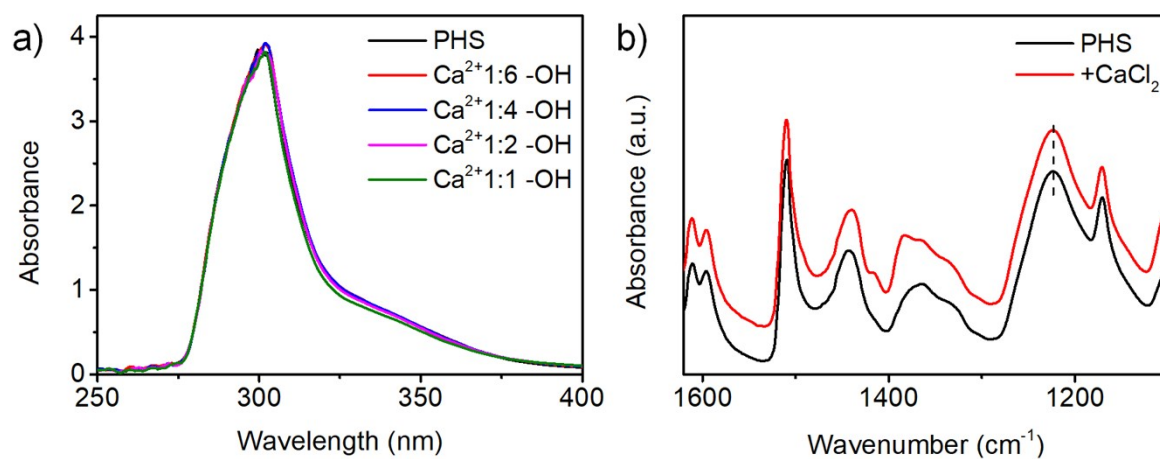


Fig. S8. **a)** UV-vis spectra of PHS in the titration experiment with different addition amount of CaCl₂. **b)** Partial FTIR spectra of PHS with the addition of CaCl₂

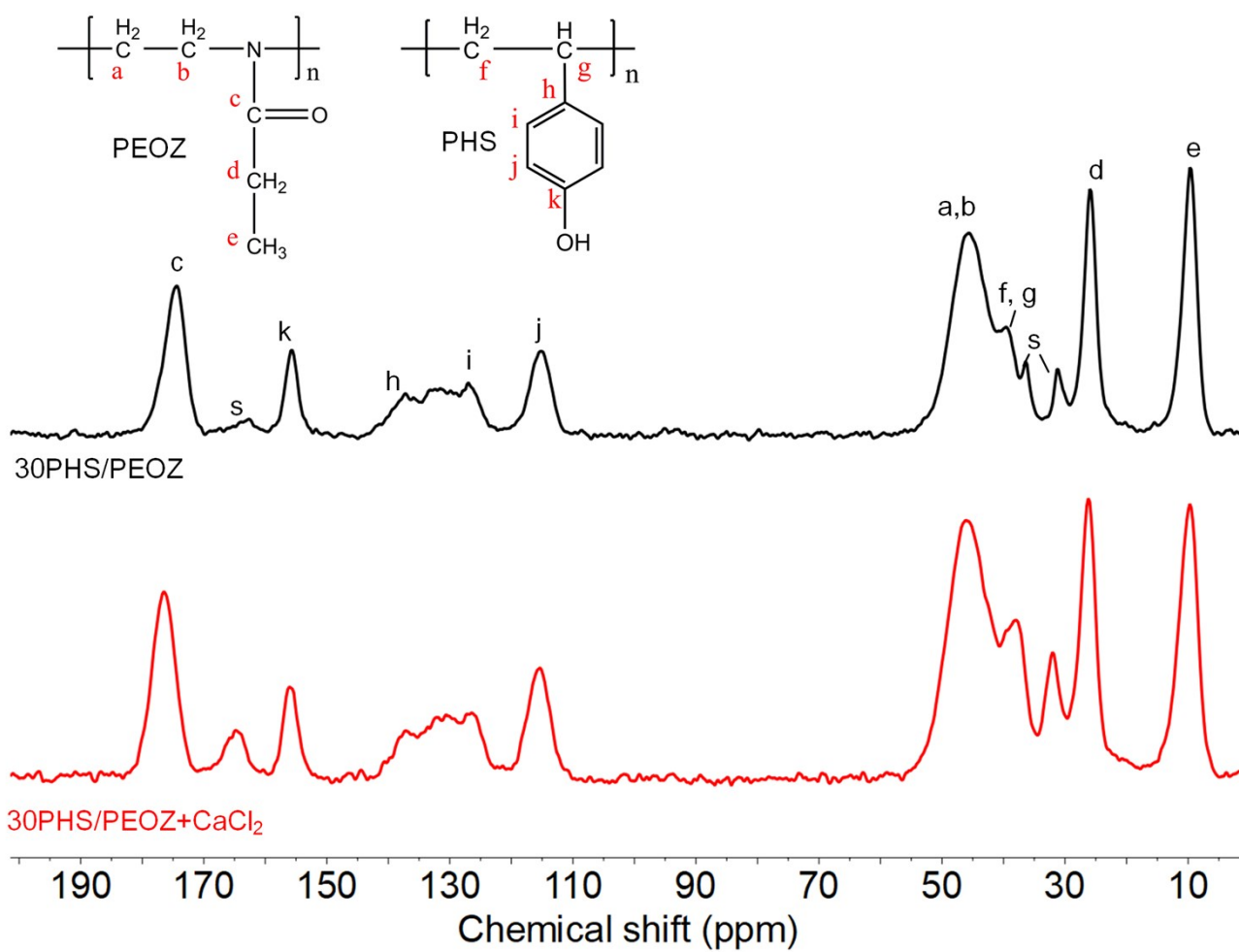


Fig. S9. Solid state ¹³C NMR spectra of 30PHS/PEOZ and 30PHS/PEOZ+CaCl₂. All peaks are assigned to the structure of PHS and PEOZ⁵. The s stands for the solvent DMF remained in the samples.

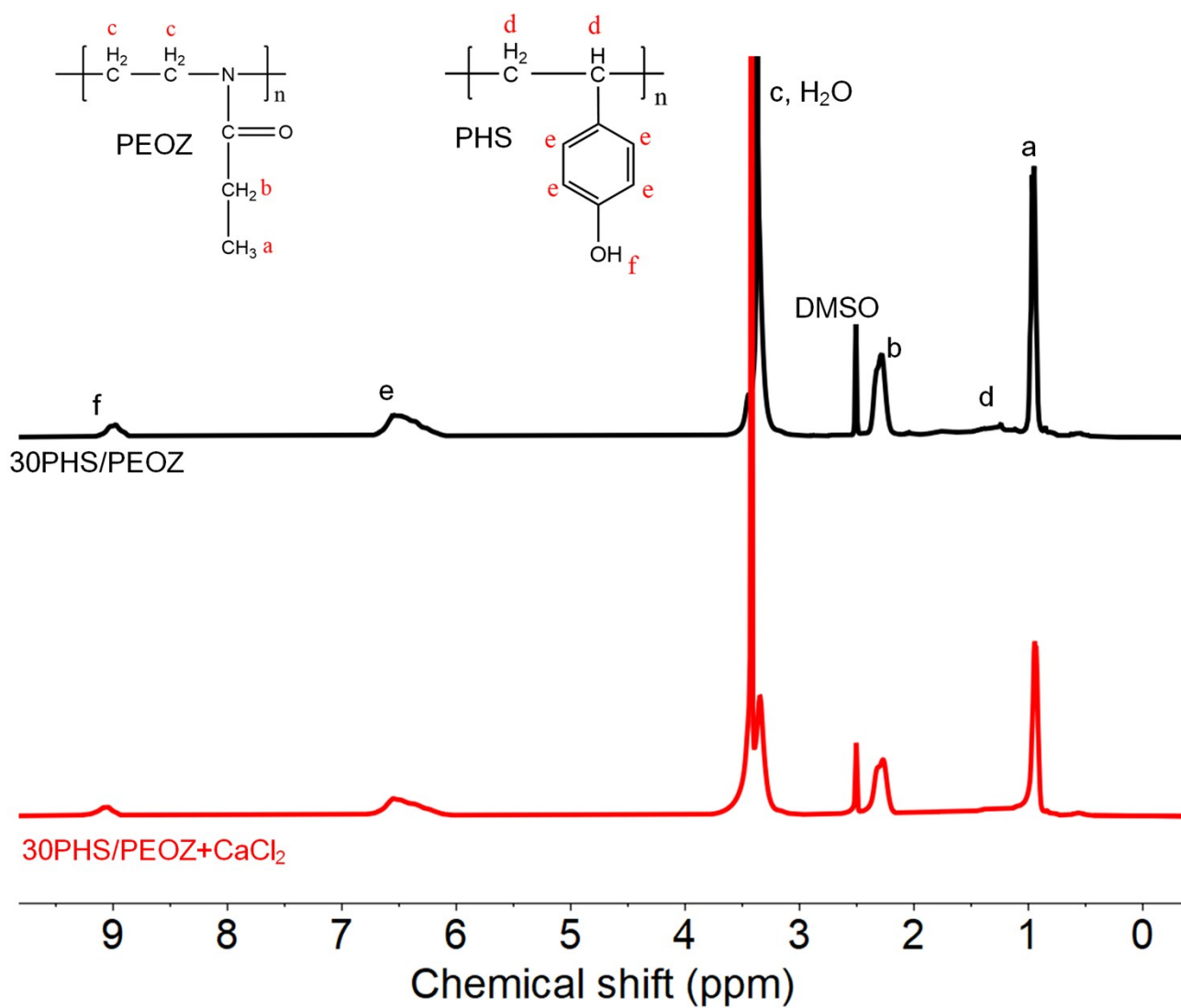


Fig. S10. ¹H NMR spectra of 30PHS/PEOZ and 30PHS/PEOZ+CaCl₂ in DMSO-d₆. Peak assignments are according to references ⁷ and ⁸.

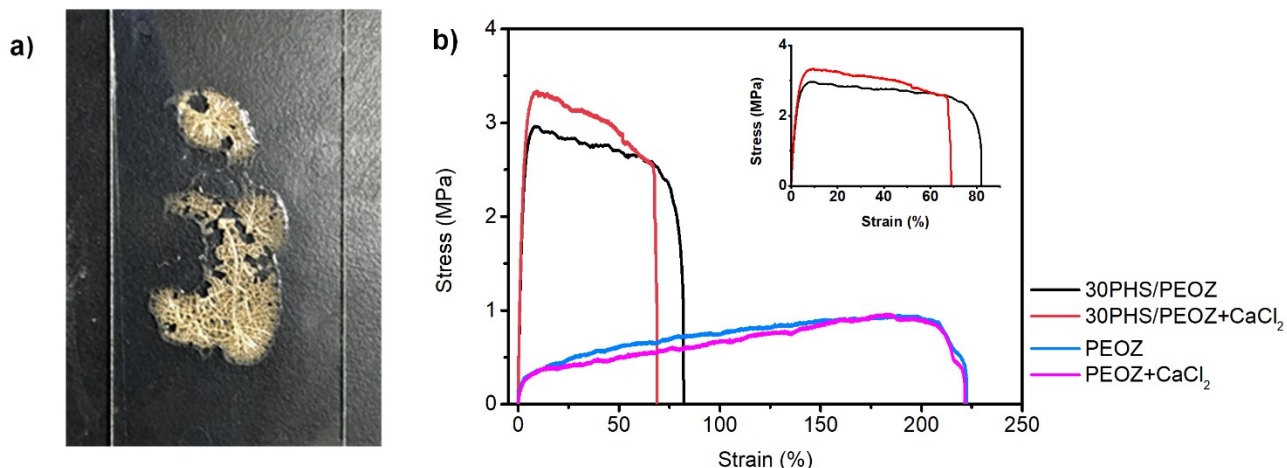


Fig. S11. a) The poor film-forming of PHS+CaCl₂. It is impossible to implement the tensile test nor even after adding CaCl₂. b) The comparisons of PEOZ vs. PEOZ+CaCl₂ and 30PHS/PEOZ vs. 30PHS/PEOZ+CaCl₂ in the tensile tests. The soft and flexible properties of PEOZ have not been modified when only the metal-ligand coordination and ionic bond exist. By comparison, the hydrogen bonds between PHS and PEOZ strengthens PEOZ obviously. On this basis, the ternary molecular interaction, which is induced by CaCl₂, further enhances the mechanical strength of PHS/PEOZ to a higher level.

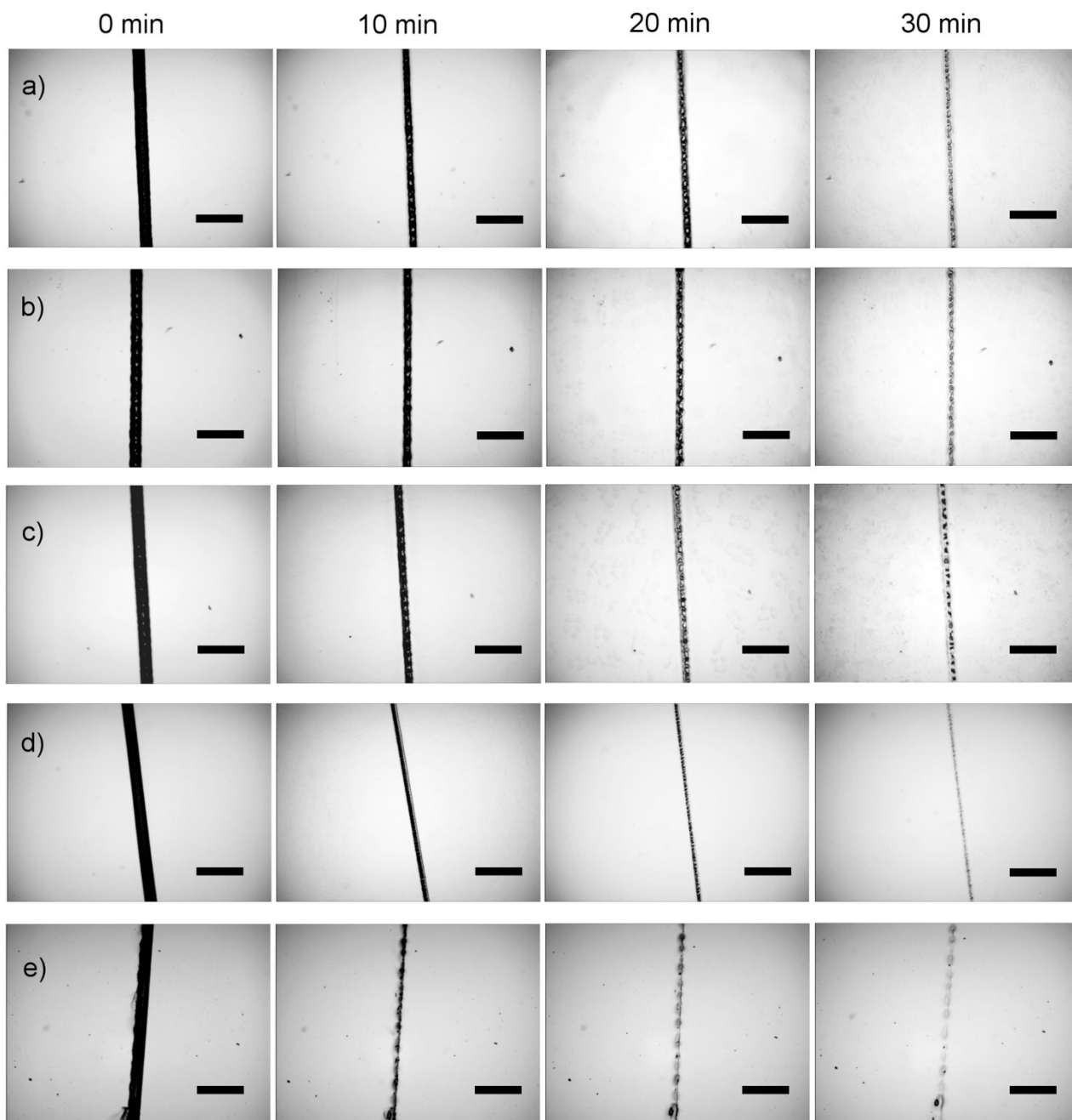


Fig. S12. Comparison of the self-healing rate among **a)** neat 30PHS/PEOZ and the blends containing **b)** $\text{Ca}(\text{NO}_3)_2$, **c)** NaCl , **d)** CaCl_2 , and **e)** MgCl_2 , respectively. Scale bars: 100 μm .

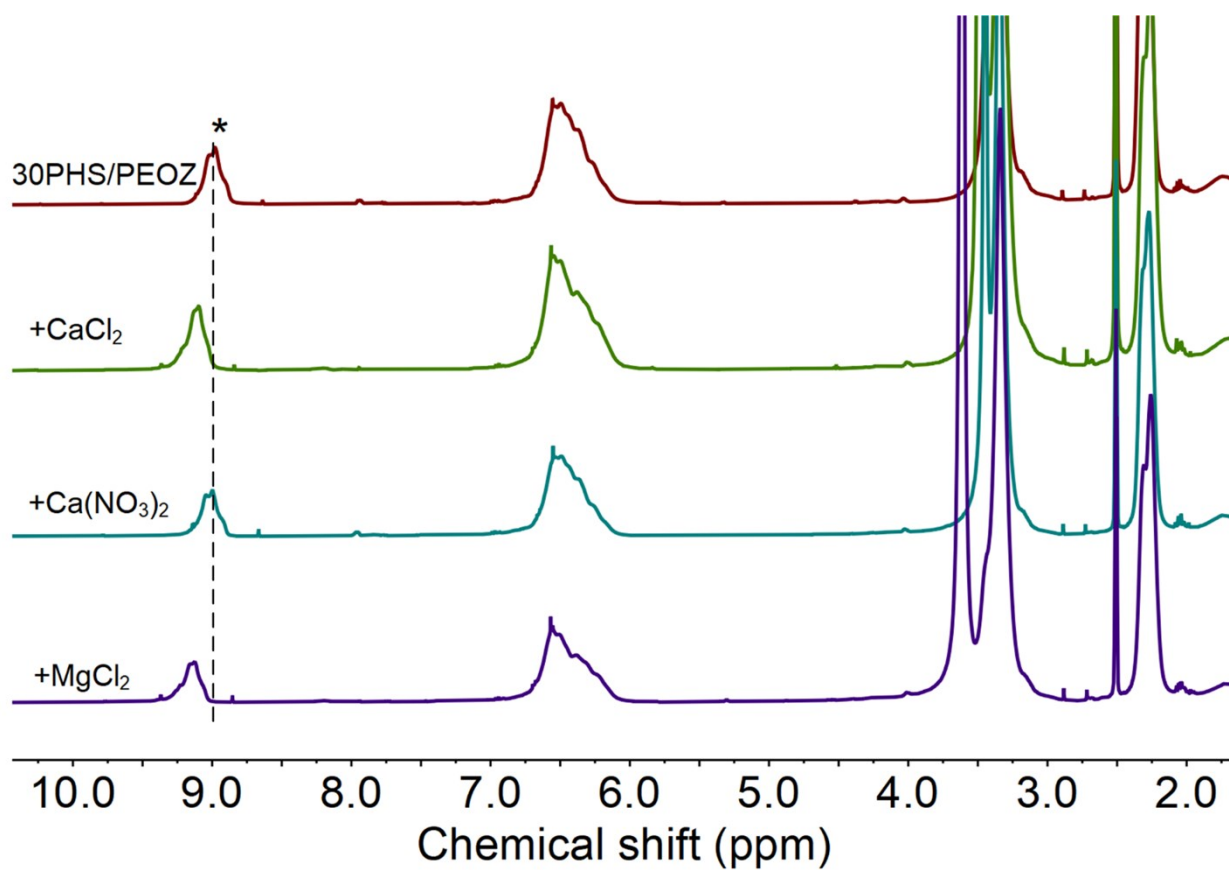


Fig. S13. ¹H NMR spectra of 30PHS/PEOZ in DMSO-d₆, and the change of the OH signal of PHS with the addition 1 equivalent of CaCl₂, Ca(NO₃)₂, and MgCl₂.

Table S2. Comparison of 30PHS/PEOZ+CaCl₂ with other self-healable coatings and films.

Motif	Transparency at 550 nm	Healing condition	Healing efficiency	Adhesion strength
This work	98.9%	RH 95%, 1 h	91.2%	2.57 MPa (0.64 MPa, RH=95%)
Poly(α -lipoic acid)/PAA/CCl/Fe ³⁺ ⁹	≤75%	14 h	86%	0.26 MPa
PVA/TA/MTM ¹⁰	85%	In water, 30 min; Water vapor, 2 h	99%	0.7 MPa
Poly(N-acryloyl 2-glycine)/hydroxyapatite ¹¹	Hydrogel	24 h	100%	0.14 MPa
Polyurethane/Disulfides ¹²	94.9%	2 h	88.2%	0.33 MPa
TA/CNC ¹³	Hydrogel	30 min	92%	15 kPa
PAA/DHA/Fe ³⁺ ¹⁴	Hydrogel	10 s	About 95% ^{a)}	32 kPa
Chitosan/PEO ₉₉ -b-PPO ₆₅ -b-PEO ₉₉ ¹⁵	Hydrogel	2 h	Nearly 100 % ^{b)}	6 kPa
PDA/talc/PAM ¹⁶	Hydrogel	30 min	60%	0.85 MPa
PVA/TA ¹⁷	Hydrogel	In water, 1 h	39.8%	90 kPa
PDA/PAM ¹⁸	Hydrogel	2 h	Nearly 100 %	15 kPa
HEMA/Aam ¹⁹	Hydrogel	15 s	80%	0.23 MPa
PPy/PEG-co-Upy ²⁰	Elastomer	5 min	100%	53 kPa

^{a)} Recovery rate of compressive strength; ^{b)} Rheological property

Table S3. The concentration of the common ions in the ancient wall paintings excavated in Shaanxi, China.

Ca	Na	Cl ⁻	NO ₃ ⁻
18.63 ug/L	3.312 ug/L	3.88 mg/L	4.57 mg/L

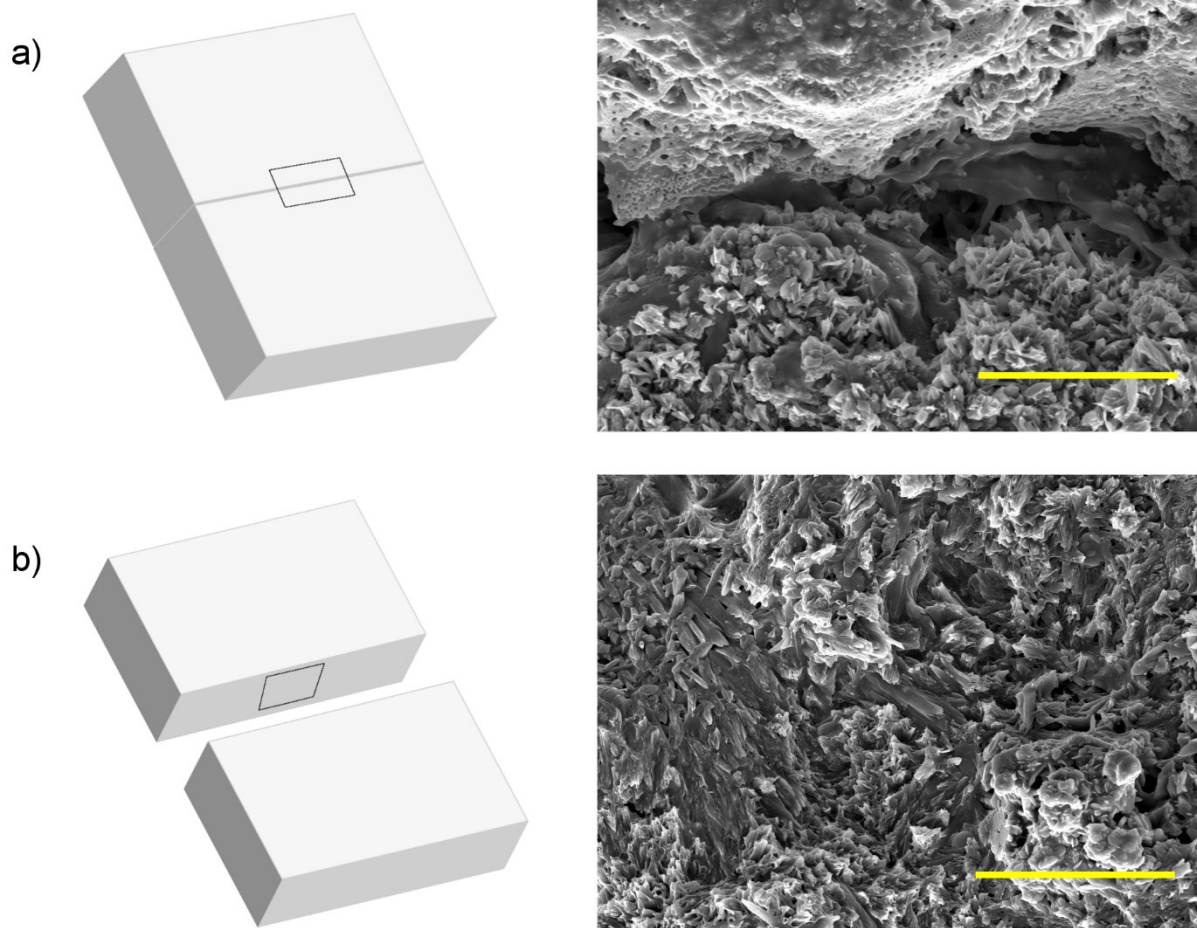


Fig. S14. SEM images of the plaster sample after the self-healing of the adhesive. **a)** The top-view from the void of the two halves. **b)** The cross-section of the fracture. Scale bars: 40 μm .

3. Supplemental references

1. D. Lin-Vien, N. B. Colthup, W. G. Fateley and J. G. Grasselli, Elsevier Science, 1991, ch. 17. Aromatic and Heteroaromatic Rings, p. 281.
2. J.-Y. Le Questel, C. Laurence, A. Lachkar, M. Helbert and M. Berthelot, *J. Chem. Soc., Perkin Trans. 2*, 1992, 2091-2094.
3. M. D. Joesten and R. S. Drago, *J. Am. Chem. Soc.*, 1962, **84**, 2696–2699.
4. T. Gramstad and W. J. Fuglevik, *Acta Chem. Scand.*, 1962, **16**, 1369-1377.
5. J. Wang, M. K. Cheung and Y. Mi, *Polymer*, 2001, **42**, 2077–2083.
6. L. M. Uriarte, J. Dubessy, P. Boulet, V. G. Baonza, I. Bihannic and P. Robert, *J. Raman Spectrosc.*, 2015, **46**, 822-828.
7. Y. Li, T. Pan, B. Ma, J. Liu and J. Sun, *ACS Appl. Mater. Interfaces*, 2017, **9**, 14429-14436.
8. Z. Yang and R. Pelton, *Macromol. Rapid Commun.*, 1998, **19**, 241-246.
9. C. Dang, M. Wang, J. Yu, Y. Chen, S. Zhou, X. Feng, D. Liu and H. Qi, *Adv. Funct. Mater.*, 2019, **29**, 1902467.
10. X. Qi, Y. Hou and M. Yang, *Adv. Funct. Mater.*, 2019, **29**, 1903984.
11. C. Cui, T. Wu, F. Gao, C. Fan, Z. Xu, H. Wang, B. Liu and W. Liu, *Adv. Funct. Mater.*, 2018, **28**, 1804925.
12. S. M. Kim, H. Jeon, S. H. Shin, S. A. Park, J. Jegal, S. Y. Hwang, D. X. Oh and J. Park, *Adv. Mater.*, 2018, **30**, 1705145.
13. C. Shao, M. Wang, L. Meng, H. Chang, B. Wang, F. Xu, J. Yang and P. Wan, *Chem. Mater.*, 2018, **30**, 3110-3121.
14. Z. Zhang, Z. Gao, Y. Wang, L. Guo, C. Yin, X. Zhang, J. Hao, G. Zhang and L. Chen, *Macromolecules*, 2019, **52**, 2531-2541.
15. J. Qu, X. Zhao, Y. Liang, T. Zhang, P. X. Ma and B. Guo, *Biomaterials*, 2018, **183**, 185-199.
16. X. Jing, H. Y. Mi, Y. J. Lin, E. Enriquez, X. F. Peng and L. S. Turng, *ACS Appl. Mater. Interfaces*, 2018, **10**, 20897-20909.
17. H. Fan, J. Wang and Z. Jin, *Macromolecules*, 2018, **51**, 1696-1705.
18. L. Han, L. Yan, K. Wang, L. Fang, H. Zhang, Y. Tang, Y. Ding, L.-T. Weng, J. Xu, J. Weng, Y. Liu, F. Ren and X. Lu, *NPG Asia Mater.*, 2017, **9**, e372.
19. R. Chen, X. Xu, D. Yu, M. Liu, C. Xiao, I. Wyman, Z. Wang, H. Yang and X. Wu, *NPG Asia Mater.*, 2019, **11**, 22.
20. J. Chen, J. Liu, T. Thundat and H. Zeng, *ACS Appl. Mater. Interfaces*, 2019, **11**, 18720-18729.